*Progress In Electromagnetics Research B, Vol. 33, 383–407, 2011*

# GENETIC ALGORITHM AND FINITE ELEMENT ANALYSIS FOR OPTIMUM DESIGN OF SLOTTED TORUS AXIAL-FLUX PERMANENT-MAGNET BRUSHLESS DC MOTOR

**A. Mahmoudi*, N. A. Rahim, and H. W. Ping**

UMPEDAC, Level 4, Engineering Tower, University of Malaya, Kuala Lumpur, Malaysia

**Abstract**—This paper presents an inside-out axial-flux permanent-magnet brushless DC motor optimized by Finite Element Analysis (FEA) and Genetic Algorithm (GA) that uses sizing equation. The double-sided slotted-stator designed TORUS motor has sinusoidal back EMF waveform and maximum power density. The GA obtained the dimensions that gave the motor its highest power density. Field analysis of the dimensions was then put through FEA, to obtain and re-optimize the motor's characteristics. Possible design parameters were investigated via use of Commercial Vector Field Opera 14.0 software used in three-dimensional FEA simulation and of MATLAB 2010a in GA programming. Techniques such as modifying winding configuration and skewing the permanent magnets were explored to achieve the most-sinusoidal back-EMF waveform and minimized cogging torque. The desired technical specifications were matched by simulation results of the 3D FEA and the GA. The FEA and the GA simulation results comparison of the flux density in different parts of the designed motor at no-load condition agreed well.

## 1. INTRODUCTION

Permanent-magnet brushless DC motors attract interest through their high performance [1]. Reduced prices of high-energy permanent magnets and electronics that the motors operate with encourage their use in a wide range of applications [2]. Brushless motors exist in various geometries; among them, a disc-type or axial-flux permanent-magnet (AFPM) motor, in various configurations [3–7]. AFPM motor's

*Received 2 July 2011, Accepted 15 August 2011, Scheduled 18 August 2011*

* Corresponding author: Amin Mahmoudi (amaminmahmoudi@gmail.com).

high torque-to-volume ratio, suitable efficiency, and flat structure attract military and transport applications, motivating researchers into developing new approaches to AFPM machine design [8]. AFPM machines can be single-sided or double-sided, with/without armature slots/core, have internal/external permanent-magnet rotors, have surface-mounted or interior permanent magnet, be single-stage or multistage [9]. Their cogging torque is usually much larger than that of conventional motors [10], but they could also earn potential to applications such as ship propulsion and elevator direct drive [11, 12]. Double-sided AFPM motors are the most promising and widely used type [13]. Topologies for double-sided AFPM machines are axial-flux one-stator-two-rotor (TORUS) and two-stator-one-rotor (AFIR) [14]; either of two arrangements (external stator or external rotor) is practical. External-stator arrangement uses few permanent magnets but at the expense of winding. External-rotor arrangement is considered particularly advantageous. Where space is limited, AFPM machine size and shape matter, and compatibility crucial. A trend in automotive and military applications is reduced size, weight, and cost [15]. Double-sided slotted TORUS AFPM motors have the most application among the other configurations; they are stronger and have higher power density [16]. Slotted TORUS AFPM motor was used here in modeling and simulation. Use of GA and FEA in the design process maximized the motor's power density and enhanced its operational performance.

Huang et al. derived the general sizing and the power density equations for radial-flux permanent-magnet machines, also a systematic method comparing capabilities of machines of various topologies [17]. In 1999, they developed the sizing equation for AFPM machines but did not present the machines' optimized sizes [18]. A general optimization process for an AFPM machine is possible with shape modification, via geometrical parameters, deterministic methods, or soft computing methods. M. Aydin presents optimum-sized AFPM machines for both TORUS and AFIR topologies, but only two parameters (diameter ratio and air-gap flux density) were considered optimization variables, the optimization via shape modification [19, 20]. In all the shape-modification methods trade-offs were observed among the performance parameters and the methods are inapplicable to multi-objective optimization problems. Soft computing methods are based on artificial intelligent techniques. Heuristic, probabilistic methods require good initial estimation, give global optimum values and are highly pliable to multi-objective optimization problems. Highly effective computer systems and new fast-computing algorithms make soft computing methods the current choices for

optimization of AFPM machines. In this paper, GA was the optimization tool minimizing AFPM machine size. Various parameters were considered, making the problem multi-objective. Note that the method is comprehensive and good for designing an arbitrary-capacity arbitrary-parameter double-sided AFPM machine; However, only slotted TORUS AFPM motor was optimized, and the equations used were for slotted TORUS AFPM motor. Between past literatures and the authors' best knowledge, minimization of AFPM machine size with various parameter considerations (winding turns, winding coefficient, electrical loading, air-gap length, diameter ratio, and air-gap flux density) has yet to be presented. There are standard techniques for optimization [21] (some of them more popular than others in electrical machines' design application): Random Search Method Hock and Jeeves Method, Powell Method, and Genetic Algorithm. Random Search Method needs a lot of time to converge and depends completely on the starting point [22]. Hook and Jeeves Method is slower than Random Search Method but is more accurate [22]. Powell Method is able to quickly reach optimal solution, but may be not robust when the problem is complicated or when the desired global minimum is hidden among many local minimums [22]. The main feature of the genetic algorithm is a population of points in parallel rather than a point to be searched [23, 24]. Many design parameters of an AFPM machine can be varied in parallel, affecting each other; the optimization is non-linear, so GA is a suitable optimization method.

Presented is the design of a slotted TORUS AFPM motor with sinusoidal back EMF and maximum power density. GA optimized it, and FEA analyzed its performance. The paper is organized as follows: sizing equation for the slotted TORUS AFPM motor was first derived in Section 2 via a generalized sizing equation, to calculate the motor's power-production potential (it was used as fitness function in the GA-optimized machine design, to minimize power-to-volume ratio); Section 3 presents the GA optimization process including design restrictions, requirements, chromosome representation, crossover, and mutation; FEA was next performed for electromagnetic field analysis of the proposed motor topology, calculating the air-gap flux distribution, verifying results from analysis of the sizing equation, all in Section 4; Section 5 discusses all the results and concludes.

## 2. SIZING EQUATION

The main dimensions of each electrical machine are determined via electrical-machine-output power equation. Assuming negligible leakage

inductance and resistance, rated power is expressed as [18]:

$$P_{out} = \eta \frac{m}{T} \int_0^T e(t) \cdot i(t) dt = m K_p \eta E_{pk} I_{pk} \tag{1}$$

$e(t)$ is phase air-gap EMF, $i(t)$ is phase current, $\eta$ is machine efficiency, $m$ is number of machine phases, and $T$ period of one EMF cycle. $E_{pk}$ and $I_{pk}$ are peaks of phase air-gap EMF and of current, respectively. $K_p$ is electrical power waveform factor, defined as:

$$K_p = \frac{1}{T} \int_0^T \frac{e(t) \cdot i(t)}{E_{pk} \cdot I_{pk}} dt = \frac{1}{T} \int_0^T f_e(t) \cdot f_i(t) dt \tag{2}$$

where $f_e(t) = e(t)/E_{pk}$ and $f_i(t) = i(t)/I_{pk}$ are expressions for normalized EMF and current waveforms. For effect of current, the current waveform factor ($K_i$) is defined as:

$$K_i = \frac{I_{pk}}{I_{rms}} = \frac{1}{\sqrt{\frac{1}{T} \int_0^T \left(\frac{i(t)}{I_{pk}}\right)^2 dt}} \tag{3}$$

where, $I_{rms}$ is phase-current $rms$ value. Table 1 lists typical waveforms and their corresponding power-waveform factor ($K_p$) and current-waveform factor ($K_i$) [25]. The peak value of phase-air-gap EMF for AFPM machine in Equation (1) is:

$$E_{pk} = K_e N_{ph} B_g \frac{f}{p} \left(1 - \lambda^2\right) D_o^2 \tag{4}$$

**Table 1.** Typical prototype waveforms.

| Model | *e(t)* | *i(t)* | $K_i$ | $K_p$ |
|---|---|---|---|---|
| Sinusoidal | 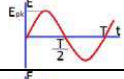 | 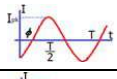 | $\sqrt{2}$ | 0.5cosφ |
| Sinusoidal | 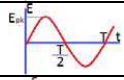 | 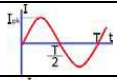 | $\sqrt{2}$ | 0.5 |
| Rectangular | 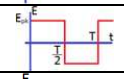 | 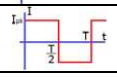 | 1 | 1 |
| Trapezoidal | 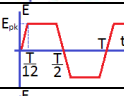 | 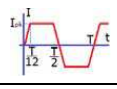 | 1.134 | 0.777 |
| Triangular | 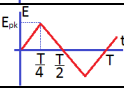 | 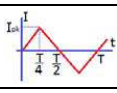 | $\sqrt{3}$ | 0.333 |

$K_e$ is EMF factor incorporating winding distribution factor ($K_w$) and per-unit portion of air-gap area-total spanned by machine's salient poles (if any); $N_{ph}$ is number of winding turns per phase; $B_g$ is flux density in air-gap; $f$ is converter frequency; $P$ is machine pole pairs; $\lambda$ is AFPM machine's diameter ratio $D_i/D_o$; $D_o$ is the diameter of machine outer surface; $D_i$ is the diameter of machine inner surface. Equation (1)'s peak phase current is:

$$I_{pk} = A\pi\, K_i \frac{1+\lambda}{2} \frac{D_o}{2m_1 N_{ph}} \tag{5}$$

where $m_1$ is the number of phases of each stator, and $A$ is the total electrical loading. A general-purpose sizing equation for AFPM machines takes the following form:

$$P_{out} = \frac{1}{1+K_\varphi} \frac{m}{m_1} \frac{\pi}{2} K_e K_i K_p K_L \eta B_g A \frac{f}{P} \left(1-\lambda^2\right) \left(\frac{1+\lambda}{2}\right) D_o^2 L_e \tag{6}$$

$L_e$ is the motor's effective axial length; $K_\varphi$ is the electrical loading ratio on rotor and stator; $K_L$ is the aspect ratio coefficient pertinent to a specific machine structure, considering effects of losses, temperature rise, and the design's efficiency requirements. Machine power density for volume total is defined as:

$$P_{den} = \frac{P_{out}}{\frac{\pi}{4} D_{tot}^2 L_{tot}} \tag{7}$$

$D_{tot}$ and $L_{tot}$ respectively are total of the machine's outer diameter and total of the machine's length including stack's outer diameter and end-winding protrusion from radial and axial iron stacks. The generalized sizing equation approach can easily be applied to a double-sided AFPM TORUS-type machine. The outer surface diameter ($D_o$) can be written as:

$$D_o = \sqrt[3]{\frac{P_{out}}{\frac{\pi\, m}{2\, m_1} K_e K_p K_i A B_g \eta \frac{f}{p} \left(1-\lambda^2\right) \left(\frac{1+\lambda}{2}\right)}} \tag{8}$$

Machine outer diameter total $D_{tot}$ for the TORUS motor is given by:

$$D_{tot} = D_o + 2W_{cu} \tag{9}$$

where $W_{cu}$ is protrusion of end winding from iron stack, in radial direction. For back-to-back wrapped winding, protrusions exist towards the machine's axis and towards its outsides, and can be calculated as:

$$W_{cu} = \frac{D_i - \sqrt{D_i^2 - \frac{2AD_{ave}}{K_{cu} J_s}}}{2} \tag{10}$$

where $D_{ave}$ is the machine's average diameter, $J_s$ is current density, and $K_{cu}$ is copper-fill factor. Machine's axial length $L_e$ is given by:

$$L_e = L_s + 2L_r + 2g \tag{11}$$

$L_r$ is rotor's axial length, and $g$ is air-gap length. Stator's axial length $L_s$ can be written as:

$$L_s = L_{cs} + 2L_{ss} \tag{12}$$

Note that for slotted machines, stator slot depth is $L_{ss} = W_{cu}$. Stator core's axial length $L_{cs}$ can be written as:

$$L_{cs} = \frac{B_g \pi \alpha_p D_o (1+\lambda)}{4pB_{cs}} \tag{13}$$

where $B_{cs}$ is stator-core flux density, and $\alpha_p$ is ratio of average-air-gap flux density to peak-air-gap flux density. Rotor's axial length $L_r$ becomes:

$$L_r = L_{cr} + L_{pm} \tag{14}$$

$L_{pm}$ is permanent-magnet length; rotor core's axial length $L_{cr}$ is:

$$L_{cr} = \frac{B_u \pi D_o (1+\lambda)}{8pB_{cr}} \tag{15}$$

where $B_{cr}$ is flux density in rotor disc core, and $B_u$ is attainable flux density on surface of permanent magnet, whose length $L_{pm}$ can be calculated as:

$$L_{pm} = \frac{\mu_r B_g}{B_r - \left(\frac{K_f}{K_d} B_g\right)} K_c g \tag{16}$$

where $\mu_r$ is magnet's recoil relative permeability, $B_r$ is permanent-magnet material residual-flux density, $K_d$ is leakage flux factor, $K_c$ is Carter factor, $K_f = B_{gpk}/B_g$ is peak-value corrected factor of air-gap flux density in radial direction of AFPM machine.

## 3. GENETIC ALGORITHM AND OPTIMIZATION

The design procedure for highest-possible-power-density AFPM motor is a multi-dimensional optimization problem of achieving a goal function within constraints. As Equations (1) to (16) show, many parameters affect each other, varying in parallel (for example: $D_i$, $D_o$, and $\lambda$); the AFPM machine's optimization is thus a non-linear problem. GA, a powerful tool, is capable of solving various complex and non-linear optimization problems [26]. It is a search algorithm inspired by life's natural-selection mechanisms and natural genetics [27, 28]. Parameters are first coded in the solution area, to

specific-length arrays (each array has a definite fitness that depends on application). GA then searches for an optimal solution; it includes chromosome representation of the solution, initializing of the first generation, cross over, and mutation [29]. In GA, inputs and their scopes of change are first determined as genes, which create the chromosomes making up a population [30]. The algorithm features a population of points in parallel rather than a point to be searched. Most of the other algorithms are not parallel and can solve the problem in just one direction, concurrently. In this case, if a solution is a local optimal solution or a subset of the original answer, all the procedures should be repeated. GA has various starting points, so it can search the solution in different directions simultaneously. If an archived solution is defeated, other available solutions could be continued and more resources are provided. In non-linear problems, variation in one parameter may have a disharmonic effect or a significant change on the whole system. Its parallelism and the various directions considered in solution selection make GA appropriate for the optimization problems with big domain and non-linearity leading to proper answer in a rather short time [31]. This property also makes GA a good option for multi-objective optimization problems because it can change many parameters simultaneously. GA may thus provide more than one answer for an optimization problem; each by considering a special parameter. There are also other methods able to expedite the solution process and improve answer accuracy; they are applicable when knowledge about domain interval increases. Another advantage of GA is that it does not need any knowledge about differentiability and can be used in noisy environments.

A difficulty in genetic algorithm programming is how to select the fitness function leading to the best solution of the problem [32]. An inappropriate fitness function may lead to the wrong answer. To select the fitness function, other parameters, too, should be considered: number of population, chromosome representation, mutation, and crossover. Another possible problem arises when one of the genes created is rather better than the other genes [33]; the answer may go towards the local solution. This is overcome by selecting a large number of populations. The following sections present the first and foremost parts of GA optimization: selection of the fitness function, number of the chromosome's genes, and design limitations.

### 3.1. Design Restrictions and Requirements

An optimum design would have maximum power density incorporated with desired sinusoidal back-EMF maintained within design restrictions and requirements. Some of the motor's parameters and charac-

teristics cannot vary much, inherently or owing to material and application limits. Besides maximum power density and sinusoidal back EMF, other limitations should be considered. Table 2 lists limits of the design procedure.

Figure 1 shows GA optimization algorithm for highest power density of the AFPM motor. GA begins with population, an initial set of random solutions. A population contains chromosomes, string-structured concatenated lists of binary digits that code the control parameters of a given problem. In this paper, a population of 1400 strings was created randomly and the chromosomes were normalized. The chromosomes evolve from generation to generation through successive iterations, each generation evaluated by a measure of fitness. Here, to create the next generation, half the genes were selected to breed a new generation, the other half eliminated. Machine power density (Equation (7)) is selected as fitness function and is in each step calculated for each chromosome. Individual solutions are fitness-selected, fitter solutions measured by the fitness function likelier to be selected. The stopping criterion is then checked; if it

**Table 2.** Design restrictions and requirements.

| **Dimensional Constraints** | |
|---|---|
| Stator Outer Diameter ($D_o$) | $D_o \leq 300\,\text{mm}$ |
| Inner to Outer Ratio ($\lambda$) | $0.4 \leq \lambda \leq 0.75$ |
| Total Axial-Length ($L_e$) | $\leq 500\,\text{mm}$ |
| Air-Gap Length ($g$) | $0.5 \leq g \leq 2.5$ |
| **Material Limitations** | |
| Stator and Rotor Core Flux Density ($B_{cs}$, $B_{cr}$) | $B_{\text{cs}}$, $B_{\text{cr}} \leq B_{\max} = 1.5\,\text{T}$ |
| Permanent Remanence | $1.3\,\text{T}$ |
| **Requirements** | |
| Rated Line-to-Line Voltage ($rms$) | $100\,\text{V} \leq$ |
| Input Phase Current ($rms$) | $\leq 20\,\text{A}$ |
| Air-gap Flux Density ($B_g$) | $0.35\,\text{T} \leq B_g \leq 0.95\,\text{T}$ |
| Electrical Loading ($A$) | $1000 \leq A \leq 30000$ |
| Output Power ($P_{nom}$) | $1\,\text{kW}$ |
| Pole Pairs ($P$) | 2 |
| Motor Efficiency ($\eta$) | $\eta \geq 80\%$ |
| Frequency ($f$) | $50\,\text{Hz}$ |
| Number of Phases ($m$) | 3 |

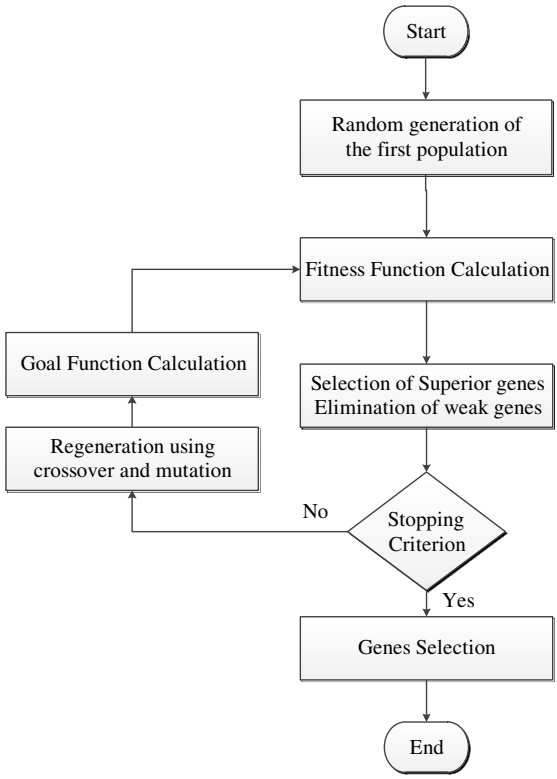


**Figure 1.** Optimization via GA.

is satisfied, the algorithm stops and the final genes are selected; else, new chromosomes called off-springs are created. New generation is formed by selecting, according to fitness value, some parents and some off-springs; others are rejected to maintain population size. Half the genes from previous steps are omitted, and new generation is created through application of crossover and mutation on selected genes. For each two selected genes, two children are created, replacing omitted genes. So, a new generation with the same population as before (1400) is created. All the previous steps are applied on the new generation, and after several generations, the algorithm is ended when the stopping criterion is satisfied. Finally, suitable selected genes give the motor optimal or near optimal dimensions for the highest power density.

### 3.2. Chromosome Representation

Genes are effective variables for fitness function and motor performance. As mentioned, many parameters affect AFPM motor


**Figure 2.** Chromosome representation ($1 \times 6$ array).

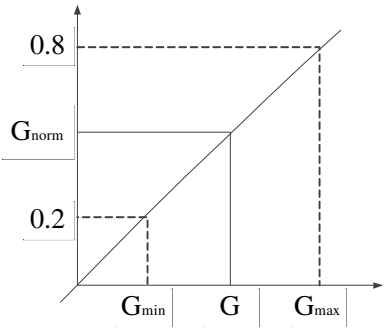


**Figure 3.** Real coding of the genes (linear normalization).

operation and they depend on each other. Fig. 2 shows the $1 \times 6$ array of each chromosome of the proposed GA; $B_g$, $\lambda$, $g$, $A$, $K_w$ and $N_{ph}$ are, respectively, air-gap flux density, inner to outer diameter ratio, air-gap length, electrical loading, winding coefficient, and winding turns in each phase. Chromosome population in each generation is 1400 and is selected randomly in the first generation.

Genes or chromosome variables are real values, so real coding is applied to each gene's normalization (see Fig. 3). Linear normalization is the result of:

$$G_{normal} = \frac{0.8 - 0.2}{G_{\max} - G_{\min}} \cdot (G - G_{\min}) + 0.2 \tag{17}$$

where $G$ is the chromosome gene varying between $G_{\min}$ and $G_{\max}$.

### 3.3. Crossover

Crossover specifies how Genetic Algorithm combines two individuals or parents to form a crossover child for the next generation. Methods of gene selection and elimination are roulette wheel selection, tournament selection, elitist selection, etc. The elitist method was used here, as selection operator for two-point crossover (see Fig. 3). Two random numbers in the interval between "1" and chromosome length "$-1$" were first generated ($1 \leq$ **Random Number** $\leq$ *chromosome length*"$-1$"). Each chromosome was then cut from the indicated points in Fig. 5, and the corresponding sections were exchanged.

### 3.4. Mutation

Mutation options specify how Genetic Algorithm makes small random changes in population individuals to create mutation children.

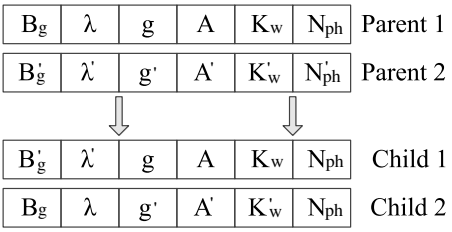


**Figure 4.** Two-point crossover.

Mutation provides genetic diversity and enables GA's search for broader space. For each method of coding, distinct mutation operators are usually defined. Mutation length is important and must be controlled. Mutation operation is executed with probability $P_m$ ($0.005 \leq P_m \leq 0.05$) and should result in a valid chromosome. For example, in real coding, genes are randomly chosen: a random value is chosen from the interval mentioned, then added to, or reduced, from the gene pool. GA uses various conditions to determine when to stop the algorithm. Presented algorithm stops when fitness function value for best current-population point is less than, or equals, fitness limit ($G_{n+1} - G_n \leq \varepsilon$). Table 2 lists each gene's optimization-allowed variations.

### 3.5. GA Results

For a 3-phase 2-pole-pair AFPM motor, possible number of slots is assumed to be 9, 12, 15, 18, 21, and 24; a program for stators with those numbers of slots was executed. The number of slots in each pole, per phase, for 9, 15, 18, and 21 slots, is fractional. Winding configuration of the fractional slot-pitch is not as easy as full slot-pitch but all the values are considered valuable because they reduce current, voltage harmonics, and cogging torque. AFPM brushless DC motor can have any even number of magnet poles ($2P$) and any number of slots ($N_s$). From this infinite set, only a small number of magnet pole and slot count combinations maximize use of stator slots and lead to efficient torque production. Appendix A presents the brushless DC AFPM motor's optimized winding configurations simulated in this paper.

Table 3 lists various parameters of the motor's design, with the different number of stator slots obtained from GA optimization. Fig. 5 shows the MATLAB-programming fitness-function variation during optimization of the various-slot-count stators [34].

**Table 3.** Dimensions of the motor, with highest power density obtained via GA.

| No. of slots | $P_{den}$ (W/cm$^3$) | $Do$ (mm) | $N_{ph}$ | $A$ (A/m) | $G$ (mm) | $L_{pm}$ (mm) | $L_{cs}$ (mm) | $L_{cr}$ (mm) | $B_g$ (mm) | $\lambda$ (mm) | $D_s$ (mm) |
|---|---|---|---|---|---|---|---|---|---|---|---|
| 9 | 0.35 | 157 | 71 | 16089 | 1.2 | 4.6 | 13.44 | 12.9 | 0.49 | 0.52 | 16.9 |
| 12 | 0.35 | 166 | 64 | 14370 | 1.07 | 2.73 | 12 | 11.7 | 0.4 | 0.46 | 16.64 |
| 15 | 0.36 | 170 | 90 | 14115 | 1.03 | 2.22 | 14 | 11 | 0.46 | 0.47 | 16 |
| 18 | 0.36 | 158 | 76 | 16757 | 1.26 | 3 | 13 | 12.5 | 0.46 | 0.55 | 17.25 |
| 21 | 0.36 | 152 | 69 | 16503 | 1.29 | 3.76 | 13.3 | 12.8 | 0.51 | 0.5 | 17.9 |
| 24 | 0.36 | 162 | 67 | 15070 | 1.21 | 2.63 | 12.99 | 12.4 | 0.46 | 0.5 | 16 |

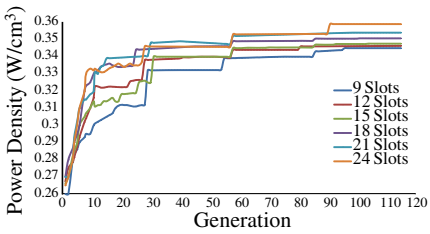


**Figure 5.** Fitness function variation during GA optimization.

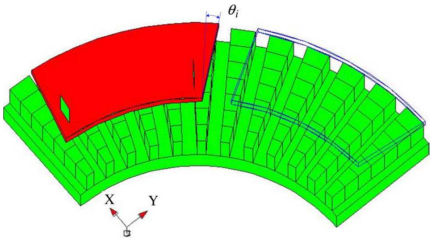


**Figure 6.** Magnet skew diagram for cogging torque and reduction of undesired harmonics.

## 4. FINITE ELEMENT ANALYSIS (FEA)

GA is used to obtain maximum power density, so dimensions obtained via GA are considered raw data; they need further analysis to be mature enough for final design. 3D FEA is used to analyze the double-sided, TORUS AFPM motor's magnetic circuit and power density, giving an overall picture of the saturation levels in various parts of the motor and extracting the motor's characteristics. Advantage of the 3D FEA approach is that different components of flux density can be calculated with high accuracy [35–39].

Usually, magnet skewing is applied to reduce cogging torque in electric machinery. It reduces back-EMF and eliminates some of the undesired harmonic components. Maximum, skewing angle should equal slot pitch, not exceed it. Fig. 6 is a diagram of the magnet's geometric skewing relative to stator teeth and slots. Skew angle $\theta_i$ is defined as the angle in which the rotor pole is skewed relative to the stator teeth. GA analysis produced stator dimensions for each slot count. FEA gave THD of the back-EMF waveform, in various

skew angles; see Fig. 7. The minimum THD was obviously for the motor with 15 slots in 9 degrees. Also, the flux density obtained from FEA was a little less than that calculated theoretically via GA, owing to core magnetic reluctance having been neglected. In real conditions, however, flux density of the different core parts decrease via MMF drop. Optimality can be possible via slight changes to magnet thickness, air-gap length, and lengths of stator yoke and rotor yoke; the best design is achieved with the utmost skill of the FEA with extreme difficulty of the changing magnet thickness, air-gap length, and lengths of stator yoke and rotor yoke, for several times. Table 4 lists the machine design's final dimensions and specifications.

Figure 8 shows only an eighth part of the motor, which was used to model the FEA-designed AFPM motor's structure: 90 degrees of the entire motor structure and 1 pole, fulfilling symmetry conditions.

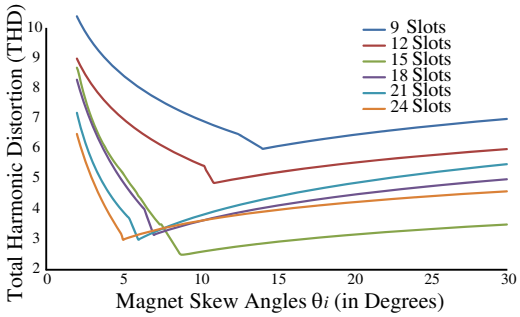


**Figure 7.** Back-EMF THD variation against skew angles for motors with different number of slots.

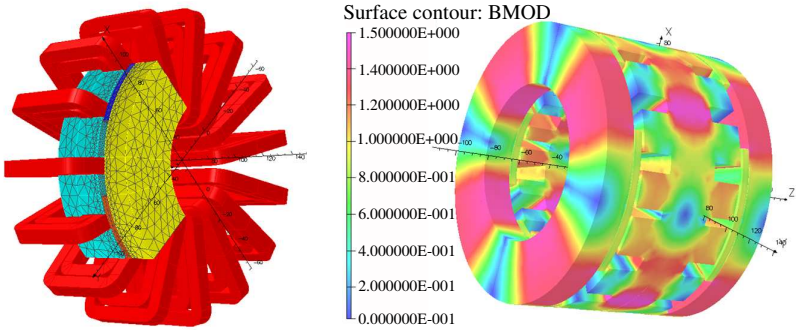


**Figure 8.** Field analysis of an AFPM motor, in vector field opera 14.0 software. (a) 3D auto-mesh generation, (b) flux-density plot.

**Table 4.** The motor's final design dimensions and specifications.

| | | |
|---|---|---|
| Nominal Voltage | $V_{nom}$ | 70 V |
| Nominal Power | $P_{nom}$ | 1 kW |
| Number of pole pairs | $P$ | 2 |
| Number of phases | $m$ | 3 |
| Drive Frequency | $f$ | 50 |
| Efficiency | $\eta$ | 87.8 % |
| Outer Diameter | $D_o$ | 170 mm |
| Inner Diameter | $D_i$ | 80 mm |
| Inner to Outer Diameter's Ratio | $\lambda$ | 0.47 |
| Magnet's axial length | $L_{pm}$ | 2.5 mm |
| Pole Pitch | $\gamma_p$ | 118° |
| Stator-yoke thickness | $2 \times L_{cs}$ | 30 mm |
| Rotor-yoke thickness | $L_{cr}$ | 11 mm |
| Slot Width | $W_s$ | 10 mm |
| Slot Depth | $D_s$ | 16 mm |
| Number of slots | $N_s$ | 15 |
| Number of winding turns per phase | $N_{ph}$ | $(15 \times 18)/3$ |
| Air-Gap Flux Density | $B_g$ | 0.47 T |
| Air-gap length | $g$ | 1 mm |

The whole machine comprises 15 slots and 2 pole-pairs. Fig. 8(a) (generated on Vector Field Opera 14.0 software) is a three-dimensional auto-mesh: tetrahedral elements with 6 nodes fitting circular shape of layers starting from shaft to outer diameter of the AFPM motor [40]. Fig. 8(b) is distribution of the magnetic flux density in different sectors of the AFPM motor.

Magnetic flux density evaluation in different sectors of an AFPM machine is important because if flux density of core or teeth goes to saturation, machine efficiency reduces, affecting operation. Fig. 9 is air-gap flux density distribution, in average radius. Maximum flux density is obviously 0.9 Tesla, averaging 0.5 Tesla.

Figure 10 shows the magnetic flux density in stator yoke and teeth at average radius. The maximum magnetic flux was 1.45 Tesla, averaging 1.2 Tesla. Fig. 11 is the magnetic flux density distribution at average rotor yoke and magnet surface radius. Table 5 lists average magnetic flux densities from the FEA simulation results and the

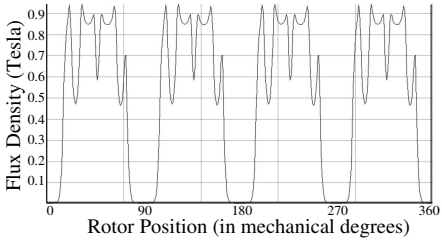


**Figure 9.** Magnetic flux density distribution of air-gap, for average radius.

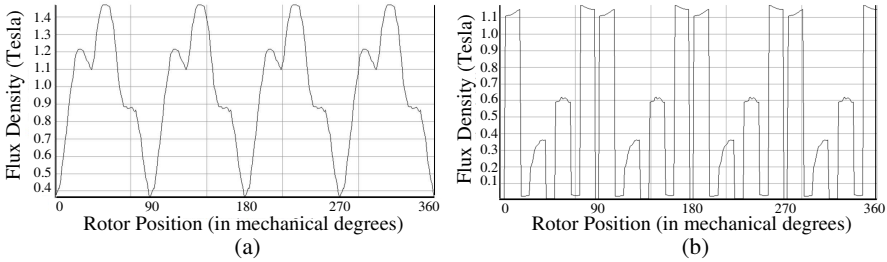


**Figure 10.** Stator magnetic flux density, for average radius. (a) Stator yoke, (b) stator teeth.

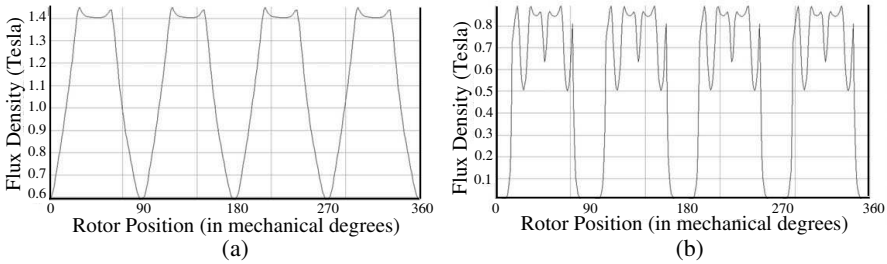


**Figure 11.** Magnetic flux density distribution for average radius, on (a) rotor yoke, (b) magnet surface.

sizing equation analysis of various parts of the motor design's no-load condition.

### 4.1. Back-EMF Waveform

The aim is to design an AFPM motor with sinusoidal waveform, i.e., the back EMF should be as sinusoidal as possible. Fig. 12 shows the back EMF at 1500 rpm, also the FEA-calculated THD and back-EMF RMS.

**Table 5.** Magnetic flux density compared among various parts of the motor, at no-load condition.

| | Air-gap | | Stator yoke | | Rotor yoke | | Magnet surface | | Teeth | | |
|---|---|---|---|---|---|---|---|---|---|---|---|
| | $B_g$ | | $B_{cs}$ | | $B_{cr}$ | | $B_m$ | | $B_t$ | | |
| | *Ave.* | *Max.* | *Ave.* | *Max.* | *Ave.* | *Max.* | *Ave.* | *Max.* | | | |
| FEA | *0.47* | *0.94* | *1.20* | *1.5* | *1.4* | *1.45* | *0.5* | *0.9* | *0.36* | *0.59* | *1.1* |
| Sizing Eq. | *0.48* | *0.95* | *1.25* | *1.5* | *1.42* | *1.48* | *0.5* | *0.9* | | | |

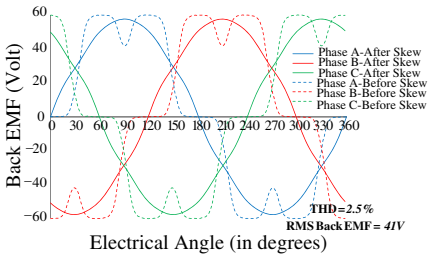


**Figure 12.** Back EMF at speed 1500 rpm.

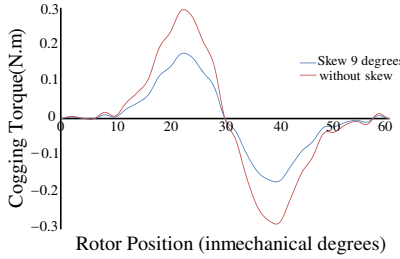


**Figure 13.** Cogging torque, with, and without, skewing.

### 4.2. Torque

Undesired torque ripple due to unwanted harmonics in output torque is one of the important concerns in designing an electric machine. Factors of undesired torque in AFPM machines are: ripple owing to permanent magnet harmonics and cogging torque. Reciprocal effect of permanent magnet and harmonic components is owed to winding distributions and current harmonic components from drive circuit. Stator's magnetic reluctance changes owing to its teeth; interaction of its magnetic reluctance with permanent magnet creates an oscillatory output torque called cogging torque, resulting from permeance difference between that of the stator teeth and slots and that of the permanent magnet. If rotor rotates freely, it stops at the position of minimum magnetic reluctance. Fig. 13 shows cogging torque of the AFPM motor with, and without, skewing. Pre-skewing, peak cogging torque was 0.29 Nm. Skewed magnets reduce cogging torque; at 9-degree skewing, peak cogging torque reduced to 0.17 Nm (a 40% reduction). Stator magnetic reluctance interaction with permanent magnet varies when stator's magnetic reluctance changes owing to teeth's presence.

### 4.3. Efficiency

For accurate assessment of machine efficiency and thermal behavior, calculation of the losses is crucial. Machine efficiency is:

$$\eta = \frac{P_{out}}{P_{out} + P_{cu} + P_{cor} + P_{rot}} \tag{18}$$

where $P_{cu}$, $P_{cor}$, $P_{rot}$ are respectively copper loss, core loss, and rotational loss components. Copper losses ($R_s \times I^2$) make up most of the loss total. Stator resistance ($R_s$) depends on load and on winding temperature [41].

$$R_s = \frac{2N_{ph\text{-}s}(l + l_e)}{\sigma_T N_{ph\text{-}p} s_{cu}} \tag{19}$$

$N_{ph\text{-}s}$ is number of winding turns in series per phase, $N_{ph\text{-}p}$ is number of winding turns in parallel per phase, $\sigma_T$ is electric conductivity of wire at temperature $T$, and $s_{cu}$ is cross-section area of wire. Thin parallel wires minimized skin effect, eliminating its consideration in Equation (19). $l$ and $l_e$ are coil length and end-winding length, respectively.

FE-AC analysis was repeated for every space harmonic component (up to the 49th order) and every current waveform's simulated time harmonic component, to get the eddy current losses in the stator steel. Core loss for stator laminated 0.1 mm thick, calculated via FE-AC analysis, was 20 W. Fig. 14 shows the motor's efficiency in various speeds. Rotational loss (which includes windage and friction losses) was estimated from [42]:

$$P_{rot} = \frac{1}{2} c_f \rho \left(\pi n^3\right) \left(D_o^5 - D_i^5\right) \tag{20}$$

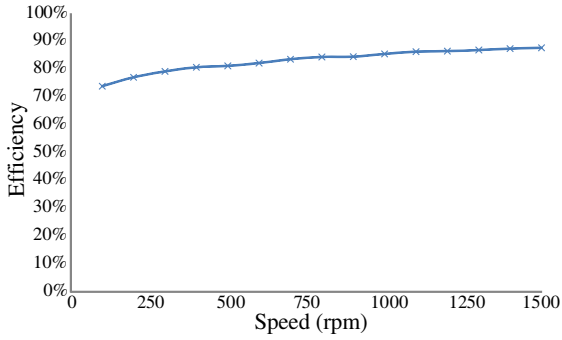


**Figure 14.** Efficiency versus speed.

where $c_f$ is friction coefficient, $\rho$ is density of the rotating part, and $n$ is rotation speed (in 'rotation per second'). Efficiency of the laminated-stator motor, obtained with full loading, was 87.8%.

## 5. CONCLUSION

Presented was an optimized AFPM brushless DC motor, the design was aided by Genetic Algorithm and Finite Element Analysis. GA sought to obtain the maximum power per volume for a 1 kW two-pole-pair AFPM slotted TORUS motor. 3D-FEA then changed and moderated the design parameters based on the electromagnetic field analysis. This approach's advantages include the capability to study different components of flux density, and to handle more complicated core and winding geometries. Different constructions and winding configurations were examined and compared and the best one was chosen. Various characteristics of the proposed design were investigated and compared with the ones desired. The simulated and the desired values agreed. Flux density of various parts of the optimal motor compared between the 3D-FEA and the sizing equation analysis, without-load, agreed. The method is comprehensive and good for designing an arbitrary-capacity arbitrary-parameter double-sided AFPM motor.

## ACKNOWLEDGMENT

The authors acknowledge University of Malaya's provision of the High Impact Research Grant No. D000022-16001 funding the Hybrid Solar Energy Research Suitable for Rural Electrification.

## APPENDIX A.

A method described in [43] was used to place the coils. There are infinite possibilities for pole and slot count combinations as there are for windings layouts; assumptions are necessary, either for focus or for scope limitation, so desirable windings can be found. The assumptions were:

a) Three-phase motor.
b) All slots filled; the number of slots is thus a multiple of the number of phases (i.e., $N_s = k \times N_{ph}$); for three-phase motors, the number of slots is thus always a multiple of three.
c) Two coil-sides in each slot, the winding can be classified as double-layer winding.

d) Balanced-windings only, i.e., only pole and slot count combinations that result in back EMF of phases B and C being $120^{oE}$ offset from back EMF of phase A.

e) Coils have equal number of turns, all spanning equal number of slots, implying same-sized coils and therefore same resistance and same inductance.

The assumptions routinely lead to motors capable of high performance, and to motors that are readily wound. Motors can be wound violating one or more of the assumptions, but they may be more difficult to wind; such winding could also lower performance. Fig. A1 shows the coil arrangements (9, 12, 15, 18, 21, and 24 slots) that gave the best sinusoidal waveforms. A, B, and C represent the phases, and + and − represent direction of the windings.

| Slot No. | 1 | 2 | 3 | 4 | 5 | 6 | 7 | 8 | 9 |
|---|---|---|---|---|---|---|---|---|---|
| up | +A | -B | -A | +B | -C | -B | +C | -A | -C |
| down | +A | +C | -A | +B | +A | -B | +C | +B | -C |

(a)

| Slot No. | 1 | 2 | 3 | 4 | 5 | 6 | 7 | 8 | 9 | 10 | 11 | 12 |
|---|---|---|---|---|---|---|---|---|---|---|---|---|
| up | +A | -B | +C | -A | +B | -C | +A | -B | +C | -A | +B | -C |
| down | +A | -B | +C | -A | +B | -C | +A | -B | +C | -A | +B | -C |

(b)

| Slot No. | 1 | 2 | 3 | 4 | 5 | 6 | 7 | 8 | 9 | 10 | 11 | 12 | 13 | 14 | 15 |
|---|---|---|---|---|---|---|---|---|---|---|---|---|---|---|---|
| up | +A | -B | +C | -A | +B | +B | -C | +A | +A | -B | +C | -A | +B | -C | -C |
| down | -B | -B | +C | +C | -A | -C | -C | +A | -B | +C | -A | -A | +B | +B | +A |

(c)

| Slot No. | 1 | 2 | 3 | 4 | 5 | 6 | 7 | 8 | 9 | 10 | 11 | 12 | 13 | 14 | 15 | 16 | 17 | 18 |
|---|---|---|---|---|---|---|---|---|---|---|---|---|---|---|---|---|---|---|
| up | +A | -B | -B | +C | -A | +B | +B | -C | +A | +A | -B | +C | +C | -A | -A | +B | -C | -C |
| down | +A | -B | +C | +C | -A | -A | +B | -C | -C | +A | -B | -B | +C | -A | +B | +B | -C | +A |

(d)

| Slot No. | 1 | 2 | 3 | 4 | 5 | 6 | 7 | 8 | 9 | 10 | 11 | 12 | 13 | 14 | 15 | 16 | 17 | 18 | 19 | 20 | 21 |
|---|---|---|---|---|---|---|---|---|---|---|---|---|---|---|---|---|---|---|---|---|---|
| up | +A | -B | -B | +C | +C | -A | -A | +B | -C | -C | +A | +A | -B | -B | +C | -A | -A | +B | +B | -C | -C |
| down | +A | -B | -B | +C | +C | -A | +B | +B | -C | -C | +A | +A | -B | +C | +C | -A | -A | +B | +B | -C | +A |

(e)

| Slot No. | 1 | 2 | 3 | 4 | 5 | 6 | 7 | 8 | 9 | 10 | 11 | 12 | 13 | 14 | 15 | 16 | 17 | 18 | 19 | 20 | 21 | 22 | 23 | 24 |
|---|---|---|---|---|---|---|---|---|---|---|---|---|---|---|---|---|---|---|---|---|---|---|---|---|
| up | +A | +A | -B | -B | +C | +C | -A | -A | +B | +B | -C | -C | +A | +A | -B | -B | +C | +C | -A | -A | +B | +B | -C | -C |
| down | +A | +A | -B | -B | +C | +C | -A | -A | +B | +B | -C | -C | +A | +A | -B | -B | +C | +C | -A | -A | +B | +B | -C | -C |

(f)

**Figure A1.** Stator winding constructions for 9, 12, 15, 18, 21, and 24 slots. (a) 9-slot double-layer stator winding (coil span = 2), (b) 12-slot double-layer stator winding (full-pitch), (c) 15-slot double-layer stator winding (coil span = 2), (d) 18-slot double-layer stator winding (coil span = 4), (e) 21-slot double-layer stator winding (coil span = 5), (f) 24-slot double-layer stator winding (full-pitch).

**Table A1.** Possible winding configurations and number of slots in each pole, per phase.

| Configuration Number | Number of Slots | Coil Pitch/Pole Pitch | Number of slots in each pole per phase ($N_{spp}$) |
|---|---|---|---|
| 1 | 9 | 2/2.25 | 0.75 |
| 2 | 12 | 2/3 | 1 |
| 3 | 12 | full-pitch | 1 |
| 4 | 15 | 2/3.75 | 1.25 |
| 5 | 15 | 3/3.75 | 1.25 |
| 6 | 18 | 3/4.5 | 1.5 |
| 7 | 18 | 4/4.5 | 1.5 |
| 8 | 21 | 3/5.25 | 1.75 |
| 9 | 21 | 4/5.25 | 1.75 |
| 10 | 21 | 5/5.25 | 1.75 |
| 11 | 24 | 4/6 | 2 |
| 12 | 24 | 5/6 | 2 |
| 13 | 24 | full-pitch | 2 |

The number of winding configuration options can also be increased by short-pitching the fractional-slot structures. The 15-slot stator was designed with a 3-slot coil span, but a 2-slot coil span is possible, reconfiguration for it easy. For an 18-slot structure, 3-slot coil span, and for 21-slot structure, both 3-slot and 4-slot coil spans can be considered. Considering the 13 stator configurations in Table A1, and possible magnet spans, their losses, back-EMF harmonic content and pulsating torque components investigated. Efficiencies were found to not differ much except at lower speeds, where the differences were more pronounced, owing to copper losses. The worst structure in terms of copper losses was found to be 24-slot full-pitched; the best was the 15-slot, either 2 or 3.75, short-pitched structure.

## APPENDIX B. NOMENCLATURE

| | | | |
|---|---|---|---|
| $A$ | electrical loading total [$A$] | $B_{cr}$ | rotor-disc flux density [T] |
| $B_{cs}$ | stator-core flux density [T] | $B_g$ | air-gap flux density [Wb/m$^2$] |
| $B_{gpk}$ | peak value of air-gap flux density [Wb/m$^2$] | $B_r$ | permanent-magnet residual-flux density [T] |
| $B_u$ | flux density on permanent-magnet surface [T] | $D_{ave}$ | machine stator average diameter [m] |

| | | | |
|---|---|---|---|
| $D_i$ | machine stator inner diameter [m] | $D_o$ | machine stator outer diameter [m] |
| $D_s$ | slot depth | $D_{tot}$ | machine outer diameter total [m] |
| $E_{pk}$ | peak value of phase-air-gap EMF | $G$ | gene value |
| $G_{\max}$ | gene maximum value | $G_{\min}$ | gene minimum value |
| $G_{normal}$ | normalized chromosome | $I_{pk}$ | phase current peak value [A] |
| $I_{rms}$ | phase current rms value $[A]$ | $J_s$ | current density [A/m$^2$] |
| $K_c$ | Carter factor | $K_{cu}$ | copper fill factor |
| $K_d$ | leakage-flux factor | $K_e$ | EMF factor |
| $K_f$ | peak value corrected factor of air-gap flux density | $K_i$ | current waveform factor |
| $K_L$ | aspect ratio coefficient | $K_p$ | electrical power waveform factor |
| $K_w$ | winding distribution factor | $K_\varphi$ | electrical loading ratio |
| $L_{cr}$ | rotor-core axial length [m] | $L_{cs}$ | stator-core axial length [m] |
| $L_e$ | effective axial length of motor [m] | $L_{pm}$ | permanent-magnet length [m] |
| $L_r$ | rotor axial length [m] | $L_s$ | stator axial length [m] |
| $L_{ss}$ | stator slot depth [m] | $L_{tot}$ | machine axial length total [m] |
| $N_{ph}$ | number of winding turns per phase | $N_{ph\text{-}p}$ | number of winding turns in parallel per phase |
| $N_{ph\text{-}s}$ | number of winding turns in series per phase | $N_s$ | Number of stator slots |
| $P$ | number of motor pole pairs | $P_{nom}$ | nominal power |
| $T$ | period of one EMF cycle [s] | $V_{nom}$ | nominal voltage |
| $W_{cu}$ | end-winding protrusion from iron stack [m] | $W_s$ | slot width |
| $c_f$ | friction coeficient | $e(t)$ | phase-air-gap EMF [V] |
| $f$ | electrical frequency [Hz] | $f_e(t)$ | normalized EMF waveforms |
| $f_i(t)$ | normalized current waveforms | $g$ | air-gap length [m] |
| $i(t)$ | phase current [A] | $l$ | coil length [m] |
| $l_e$ | end winding length [m] | $m$ | number of machine's phases |
| $m_1$ | number of phases of each stator | $n$ | rotation speed [rs$^{-1}$] |
| $s_{cu}$ | cross-section area of wire [m$^2$] | $\alpha_p$ | average air-gap flux density to its peak value ratio |
| $\gamma_p$ | pole pitch | $\eta$ | motor efficiency |
| $\theta_i$ | permanent magnet skew [in degrees] | $\lambda$ | diameter ratio |
| $\mu_r$ | recoil relative permeability of magnet | $\rho$ | density [kg/m$^3$] |
| $\sigma_T$ | electric conductivity of wire [S/m] | | |

## REFERENCES


1. Hadef, M., M. R. Mekideche, A. Djerdir, and A. Miraoui, "An inverse problem approach for parameter estimation of interior permanent magnet synchronous motor," *Progress In Electromagnetics Research B*, Vol. 31, 15–28, 2011.
2. Touati, S., R. Ibtiouen, O. Touhami, and A. Djerdir, "Experimental investigation and optimization of permanent magnet motor based on coupling boundary element method with permeances network," *Progress In Electromagnetics Research*, Vol. 111, 71–90, 2011.
3. Cho, C. P. and B. K. Fussel, "Detent torque and axial force effect in a dual air-gap axial-field brushless motor," *IEEE Transaction on Magnetics*, Vol. 6, 2416–2418, November 1993.
4. Mendrela, E. A., R. Beniak, and R. Wrobel, "Influence of stator structure on electromechanical parameters of torus-type brushless DC motor," *IEEE Transaction on Energy Conversion*, Vol. 18, No. 2, 231–237, June 2003.
5. Lukaniszyn, M., M. Jagiela, and R. Wrobel, "A disc-type motor with co-axial flux in the stator-influence of magnetic circuit parameters on the torque," *Electrical Engineering*, Vol. 84, No. 2, 61–71, 2002.
6. Chalmers, B. J. and E. Spooner, "An axial-flux permanent-magnet generator for a gearless wind energy system," *IEEE Transaction on Energy Conversion*, Vol. 14, 251–257, June 1999.
7. Barakat, G., T. El-Meslouhi, and B. Dakyo, "Analysis of the cogging torque behavior of a two-phase axial flux permanent magnet synchronous machine," *IEEE Transaction on Magnetics*, Vol. 37, 2803–2805, July 2001.
8. Liu, C. T. and S. C. Lee, "Magnetic field modeling and optimal operational control of a single-side axial-flux permanent magnet motor with center poles,"*Journal of Magnetism and Magnetic Materials*, Vol. 304, No. 1, 454–456, September 2006.
9. Mahmoudi, A., N. A. Rahim, and W. P. Hew, "Axial-flux permanent-magnet machine modeling, design, simulation, and analysis," *Scientific Research and Essay (SRE)*, Vol. 6, No. 12, 2525–2549, June 2011.
10. Barakat, G., T. El-meslouhi, and B. Dakyo, "Analysis of the cogging torque behavior of a two-phase axial flux permanent magnet synchronous machine," *IEEE Transaction on Magnetics*, Vol. 37, No. 4, 2803–2805, July 2001.

11. Caricchi, F., F. Crescimbini, and O. Honrati, "Modular axial-flux permanent-magnet motor for ship propulsion drives," *IEEE Transaction on Energy Conversion*, Vol. 14, No. 3, 673–679, September 1999.
12. Ficheux, R. L., F. Caricchi, F. Crescimbini, and O. Honorati, "Axial-flux permanent-magnet motor for direct-drive elevator systems without machine room," *IEEE Transaction on Industry Applications*, Vol. 37, No. 6, 1693–1701, November–December 2001.
13. Gieras, J. F., R. J. Wang, and M. J. Kamper, *Axial Flux Permanent Magnet Brushless Machines*, Springer Verla, 2008.
14. Mahmoudi, A., N. A. Rahim, and W. P. Hew, "TORUS and AFIR axial-flux permanent-magnet machines: a comparison via finite element analysis," *International Review on Modelling and Simulations*, Vol. 4, No. 2, 624–631, April 2011.
15. Liu, C. T., S. C. Lin, and T. S. Chiang, "On the analytical flux distribution modeling of an axial-flux surface-mounted permanent magnet motor for control applications original research," *Journal of Magnetism and Magnetic Materials*, Vol. 282, 346–350, November 2004.
16. Gholamian, S. A., "Optimum design and manufacturing of axial flux permanent magnet motor for electric vehicle application," Ph.D. Dissertation, K. N. Toosi Univ. Technology, Tehran, Iran, January 2008.
17. Huang, S., J. Luo, F. Leonardi, and T. A. Lipo, "A general approach to sizing and power density equations for comparison of electrical machines," *IEEE Transaction on Industry Applications*, Vol. 34, No. 1, 92–97, January–February 1998.
18. Huang, S., J. Luo, F. Leonardi, and T. A. Lipo, "A comparison of power density for axial flux machines based on the general purpose sizing equation," *IEEE Transaction on Energy Conversion*, Vol. 14, No. 2, 185–192, January 1999.
19. Aydin, M., S. Huang, and T. A. Lipo, "Design and 3D electromagnetic field analysis of non-slotted and slotted TORUS type axial flux surface mounted permanent magnet disc machines," *IEEE International Electric Machines and Drives Conference*, January 17–20, 2001.
20. Aydin, M., S. Huang, and T. A. Lipo, "Optimum design and 3D finite element analysis of nonslotted and slotted internal rotor type axial flux PM disc machines," *IEEE Power Engineering Society Summer Meeting*, July 15–19, 2001.
21. Rao, S. S., *Optimization: Theory and Application*, Wiley Eastern Limited, New Delhi, 1985.

22. Rao, S. S., *Engineering Optimization: Theory and Practice*, Wiley, 1996.
23. Pemha, E. and E. Ngo Nyobe, "Genetic algorithm approach and experimental confirmation of a laser-based diagnostic technique for the local thermal turbulence in a hot wind tunnel jet," *Progress In Electromagnetics Research B*, Vol. 28, 325–350, 2011.
24. Gen, M. and R. Cheng, *Genetic Algorithms and Engineering Optimization*, Wiley, New York, 2000.
25. Rahim, N. A., W. P. Hew, and A. Mahmoudi, "Axial-flux permanent-magnet brushless dc traction motor for direct drive of electric vehicle," *International Review of Electrical Engineering*, Vol. 6, No. 2, 760–769, April 2011.
26. Tokan, F. and F. Gunes, "The multi-objective optimization of non-uniform linear phased arrays using the genetic algorithm," *Progress In Electromagnetics Research B*, Vol. 17, 135–151, 2009.
27. Goldberg, D. E., *Genetic Algorithms in Search, Optimization & Machine Learning*, Addison-Wesley, January 1989.
28. Conn, A. R., N. I. M. Gould, and L. Toint, Ph., "A globally convergent augmented lagrangian algorithm for optimization with general constraints and simple bounds," *SIAM Journal on Numerical Analysis*, Vol. 28, No. 2, 545–572, April 1991.
29. Conn, A. R., N. I. M. Gould, and Ph. L. Toint, "A globally convergent augmented lagrangian barrier algorithm for optimization with general inequality constraints and simple bounds," *Mathematics of Computation*, Vol. 66, No. 217, 261–288, January 1997.
30. Üler, G. F., O. A. Mohammed, and C. S. Koh, "Utilizing, genetic algorithms for the optimal design of electromagnetic devices," *IEEE Transactions on Magnetics*, Vol. 30, No. 6, November 1994.
31. Üler, G. F., O. A. Mohammed, and C. S. Koh, "Design optimization of electrical machines using genetic algorithms," *IEEE Transactions on Magnetics*, Vol. 31, No. 3, May 1995.
32. Wurtz, F., M. Richomme, J. Bigeon, and J. C. Sabonnadiere, "A few results for using genetic algorithms in the design of electrical machines," *IEEE Transactions on Magnetics*, Vol. 33, No. 2, May 1997.
33. Mirzaeian, B., M. Moallem, V. Tahani, and C. Lucas, "Multiobjective optimization method based on a genetic algorithm for switched reluctance motor design," *IEEE Transactions on Magnetics*, Vol. 30, No. 3, May 2002.

34. MATLAB 2010a, User Guide, MathWorks Inc., 2010, http://www.mathworks.com.
35. Mahmoudi, A., N. A. Rahim, and W. P. Hew, "Analytical method for determining axial-flux permanent-magnet machine sensitivity to design variables," *International Review of Electrical Engineering*, Vol. 5, No. 5, 2039–2048, September–October 2010.
36. Vaseghi, B., N. Takorabet, and F. Meibody-Tabar, "Transient finite element analysis of induction machines with stator winding turn fault," *Progress In Electromagnetics Research*, Vol. 95, 1–18, 2009.
37. Torkaman, H. and E. Afjei, "FEM analysis of angular misalignment fault in SRM magnetostatic characteristics," *Progress In Electromagnetics Research*, Vol. 104, 31–48, 2010.
38. Torkaman, H. and E. Afjei, "Comparison of two types of dual layer generator in field assisted mode utilizing 3D-FEM and experimental verification," *Progress In Electromagnetics Research B*, Vol. 23, 293–309, 2010.
39. Torkaman, H. and E. Afjei, "Magnetio static field analysis regarding the effects of dynamic eccentricity in switched reluctance motor," *Progress In Electromagnetics Research M*, Vol. 8, 163–180, 2009.
40. Opera Version 14.0 User Guide, Vector Fields, 2011, http://www.cobham.com.
41. Wang, R. J., M. J. Kamper, and K. V. D. Westhuizen, "Optimal design of a coreless stator axial flux permanent magnet generator," *IEEE Transaction on Magnetics*, Vol. 41, No. 1, 55–64, January 2005.
42. Saari, J., "Thermal analysis of high-speed induction machines," Ph.D. Dissertation, Helsinki Univ. Technology, Helsinki, Finland, January 1998.
43. Hanselman, D. C., *Brushless Permanent Magnet Motor Design*, McGraw-Hill, New York, 1994.